Available online at www.sciencedirect.com
ScienceDirect
Journal of Colloid and Interface Science 315 (2007) 562–568
JOURNAL OF Colloid and Interface Science
www.elsevier.com/locate/jcis

# Cerium modified MCM-41 nanocomposite materials via a nonhydrothermal direct method at room temperature

Kamal Mohamed Sayed Khalil

*Chemistry Department, Faculty of Science, Sohag University, P.O. Box 82524, Sohag, Egypt*

Received 18 May 2007; accepted 13 July 2007

Available online 21 July 2007

**Abstract**

Ce-containing MCM-41 materials were prepared via a direct, nonhydrothermal method at room temperature from *tetra*-ethoxysilane, *n*-hexadecyl trimethyl ammonium bromide, ammonia solution, and cerium(IV) ammonium nitrate precursors. Composite materials containing the nominated ratios of 5 and 10% (w/w) $CeO_2$/MCM-41 were targeted. The obtained materials were investigated by TGA, DSC, FTIR, diffuse reflectance UV–vis, XRD, $N_2$ adsorption/desorption isotherms, and SEM. Results indicated the insertion of cerium ions in tetrahedral environment in the framework of MCM-41. BET surface area amounting to 824 and 726 $m^2/g$; total pore volume amounting to 0.427 and 0.515 $cm^3/g$; and narrow pore size distribution maximizing at 22.5 and 23.7 Å, respectively were obtained for the 5 and 10% $CeO_2$/MCM-41 calcined composites. SEM showed a spherical type morphology for the composites which is rather similar to their blank MCM-41, and no clear ceria aggregates were observed on the external surfaces of composites spherical particles. Thus, the adopted method allows the persistence of MCM-41 texture with cerium inserts in the framework of MCM-41 and/or forms finely divided ceria nanoparticles on the wall of MCM-41 materials. Moreover, stabilization of any formed ceria nanoparticles was attributed to the short nonintersecting porous nature of MCM-41 matrix, which hinders their aggregation upon calcinations.


*Keywords:* MCM-41; Ce-MCM-41; $CeO_2$; Mesoporous; Composite material

## 1. Introduction

Since the discovery of ordered mesoporous materials in the early 1990s [1,2], MCM-41 type of materials have capture great interest due to their high surface area (>1000 $m^2/g$), regular pore system (hexagonally shaped pores with a uniform size of 2–10 nm in nonintersecting straight channels), and high thermal stability [3,4].

Similar to zeolites, ordered mesoporous silica materials do not often utilize as catalysts as such. Thus, it is a common practice to modify these materials via introduction of additional reactive species [5]. Therefore, synthesis and characterization of ordered mesoporous materials of modified surfaces for application as host materials and as catalysts present a very attractive area for recent researches [6–11]. Modification of ordered mesoporous materials can be approached via different possible pathways which include: post-synthesis modification of the as prepared (uncalcined) [6–8], or the calcined [9,10] mesoordered materials, as well as direct modification [11] during synthesis. Moreover, due to the textural advantages of MCM-41 materials, incorporation of catalytic active species/and or nanoparticles offers attractive approach for the preparation of innovative catalysts composed of metals and/or metal oxides in MCM-41 matrices. For examples preparation of $TiO_2$/MCM-41 and $V_2O_5/TiO_2$/MCM-41 [12], MCM-41 containing zirconium and manganese ions (Zr-Mn-MCM-41) [13], and ZnO/MCM-41 [14] have been investigated.

Cerium containing materials are very important and interesting class of materials [15–17]. In particular, cerium containing MCM-41 materials are very interesting and find many catalytic applications in vapor-phase dehydration of cyclohexanol and hydroxylation of 1-naphthol with aqueous $H_2O_2$ and *tert*-butyl hydroperoxide [18]; in selective acylation and alkylation reaction [19]; in liquid oxidation of cyclohexane to cyclohexanol

*E-mail address:* kms_khalil@yahoo.co.uk.

0021-9797/$ – see front matter 
doi:10.1016/j.jcis.2007.07.030

[20]; and for *n*-heptane oxidation [21] where, incorporation of cerium to MCM-41 was found to improve hydrothermal stability and enhance the adsorption and catalytic properties.

Laha et al. [18], have prepared Ce containing MCM-41 by hydrothermal methods from fumed silica and ceric sulfate precursors. Similar hydrothermal preparation from fumed silica and cerium chloride precursor was reported by Araujo et al. [21]. However, Kadgaonkar et al. [19] have carried out hydrothermal synthesis of Ce-MCM-41 by refluxing the gel with magnetic stirring under atmospheric pressure for 24–36 h. Yao et al. [20] have prepared Ce-MCM-41 from tetraethyl orthosilicate (TEOS) and ($Ce(NO_3)_3{\cdot}6H_2O$) precursors in presence of a cationic surfactant (CTAB) and NaOH. The final mixture was subjected for stirring (for 24 h) and hydrothermal treatment under autogenous pressure without stirring at 363 K for 7 days.

A novel synthesis route was introduced by Gürn et al. [22] for the preparation of mesoporous MCM-41 materials. This route is based on the use of tetra-*n*-alkoxysilanes such as tetraethoxysilane (TEOS) as a silica source which are added to an aqueous solution of a cationic surfactant in the presence of ammonia as a catalyst. Moreover, the reaction mixture can be homogenized with ethyl alcohol to facilitate the formation of spherical MCM-41 particles. Based on Gürn et al. method [22], preparation of Al-MCM-41 [23], Ti-MCM-41 [24–26], and Ni-MCM-41 [27] at room temperature recently have been reported. The present article describes a nonhydrothermal, and direct method for the preparation of cerium modified MCM-41 materials at room temperature. $CeO_2$/MCM-41 composite containing the nominated ratios 5 and 10% (w/w) were targeted and characterized via different techniques. The present method is suitable for fast preparation of small or large batches of spherical $CeO_2$/MCM-41 particles.

## 2. Experimental

### 2.1. Preparation

#### 2.1.1. Chemicals

*n*-Hexadecyltrimethylammonium bromide (C16TMABr), 98% Aldrich; tetraethoxysilane (TEOS), 98% $Si(OC_2H_5)_4$, Sigma–Aldrich; cerium(IV) ammonium nitrate $(NH_4)_2Ce(NO_3)_6$, Aldrich; ammonia solution, $NH_4OH$ (25% $NH_3$), 99.99%, Merck; and ethyl absolute alcohol, $C_2H_5OH$, analytical grade product supplied by Alfa Acer, were purchased and used as received. All preparation were carried out at room temperature which was controlled at $22 \pm 1\,^{\circ}C$.

#### 2.1.2. Preparation of blank MCM-41 silica

Following the procedure described by Grün et al. [22], 0.007 mol of the cationic surfactant (C16TMABr) was dissolved in 50 ml of deionized water, and 17 ml of ammonia solution was added (0.25 mol) to the surfactant solution followed by 76 ml of ethanol. The solution was stirred and 5.0 ml of TEOS (0.022 mol) was added. After 2 h of stirring at 400 r.p.m. the resulted gel was filtered, washed, and dried for 24 h at 90 °C. This dried product was termed as the *uncalcined* MCM-41 *material.* Portion of the latter was heated at 1 °C/min up to 550 °C and kept at this temperature for 3 h, the produced material was termed as the *calcined* MCM-41 *material*.

#### 2.1.3. Preparation of ceria modified MCM-41 silica

A modified preparation method was adopted to allow direct incorporation of cerium species in the MCM-41 material at room temperature. Thus, 0.007 mol of the cationic surfactant (C16TMABr) was dissolved in 50 ml of deionized water and 17 ml of ammonia solution was added to the surfactant solution followed by 76 ml of ethanol. The solution was stirred (at 400 r.p.m.) and 5.0 ml of TEOS was added followed by 0.210 g of cerium(IV) ammonium nitrate (corresponding to 5% (w/w) $CeO_2$/silica) thus a yellowish clear solution was obtained. After stirring for 30 min, 17 ml (0.25 mol) of ammonia solution was added under continuous stirring. The reaction mixture turned turbid (in one minute time), then a bright yellow colloidal gel was formed. After 2 h of continuous stirring, the resulted gel was filtered, washed, and dried for 24 h at 90 °C. The latter product was termed as the *uncalcined* 5% $CeO_2$/MCM-41 composite material. Similar preparation was made by increasing of the amount of cerium(IV) ammonium nitrate to correspond to 10% (w/w) $CeO_2$/silica. The product obtained after drying at 90 °C was termed as the *uncalcined* 10% $CeO_2$/MCM-41 composite material. Portion of the uncalcined composite materials were heated at 1 °C/min up to 550 °C and kept at this temperature for 3 h, the produced materials were termed as the *calcined* 5%, and 10% $CeO_2$/MCM-41 composite materials.

### 2.2. Characterization

#### 2.2.1. Thermal analyses

A Thermal Analyst 2000 TA instrument (USA) controlling a 2050 thermogravimetric analyzer (TGA) and 2010 differential scanning calorimeter (DSC) was used. For TGA measurements, a ceramic sample boat was used with samples weighing $5.0 \pm 0.1$ mg. Data recorded upon heating up to 700 °C at 2 °C/min and in a stream (40 ml/min) of air, or nitrogen gas as indicated. For DSC measurements, a sample size of $5.0 \pm 0.1$ mg was heated up to 550 °C in a covered aluminum sample pan at 10 °C/min and a flow of 40 ml/min of nitrogen gas.

#### 2.2.2. FTIR spectroscopy

FTIR spectra for the test materials were carried out using KBr disc technique using an FTIR spectrometer, model Shimadzu-FTIR800 (Japan), in the range 4000–400 $cm^{-1}$, with 40 scans and a resolution of 4 $cm^{-1}$.

#### 2.2.3. Diffused reflectance

(DR) UV–vis spectroscopy: DR UV–vis spectra for the calcined materials were obtained using a Shimadzu model 2100 spectrophotometer (Japan). $BaSO_4$ was used as a reference material.

#### 2.2.4. X-ray diffraction (XRD)

XRD patterns were obtained using a Philips 1840 diffractometer at room temperature using Cu$K_\alpha$ radiation. Diffrac-

tion patterns were obtained with Ni-filtered Cu$K_\alpha$ radiation ($\lambda = 0.15418$ nm). The resultant patterns matched with standard data for $CeO_2$ [28] for the purpose of phase identification.

*2.2.5. Scanning electron microscopy (SEM)*

SEM micrographs were obtained, using a Jeol Microscope Model JSM-5600 (Japan). The samples were coated with gold before investigation.

*2.2.6. Nitrogen gas adsorption*

Nitrogen adsorption/desorption isotherms at 77 K were measured according to the recommendations of the IUPAC [29] using a model 100 Autosorb, Quantachrome Instrument Corporation (USA). Prior to measurement, all samples were degassed for 2 h at 250 °C to 0.1 Pa. Specific surface area, $S_{BET,}$ was calculated using the BET equation [30]. Total pore volume, $V_p$ was calculated at $P/P_0 = 0.95$. The pore width, $P_w$ distribution over the range of ∼(2–80 nm) was generated from the adsorption branches of the isotherms via BJH method [31]. Calculations, were performed using Autosorb 1 software for windows (copyright, 1995–2003, Quantachrome Instruments).

## 3. Results and discussion

Fig. 1 shows TGA and DTG curves for the uncalcined blank MCM-41 in flow of $N_2$ atmosphere (top) and in flow of air (bottom). Total weight loss, recorded upon heating over the temperature range of *RT*–700 °C was 41.9% in $N_2$ flow (or 43.6% in flow of air). The results show that weight loss process and evolution of the MCM-41 structure occurred through a four steps process, as shown in Table 1. The steps limits and weight loss values for each sample were very sensitive for the type of atmosphere ($N_2$ gas or air). Based on the thermal analysis studies reported for similar systems [32], the first step below 120 °C is assignable for the loss of the adsorbed and included water molecules and/or organic. This followed by two steps maximize at 235 °C, 390 °C in flow of $N_2$ atmosphere, (or at 225 and 280 °C in flow of air). These two steps, together, represent the major portion of the weight loss process (37.5 out of 41.9% in flow of $N_2$, and 36.6 out of 43.6% in flow of air) and they are mainly assignable for the removal of the template. Finally, the fourth step of the weight loss process, above 550 °C, shows a small weight loss amounting to <0.1% either in flow of $N_2$ gas or air. These results are in agreement with the reported mechanism for template removal that based on Hofmann degradation at low temperature below 250 °C, which followed by decomposition and/or combustion reaction above 250 °C [32]. Thus, the peak observed at 390 °C (in $N_2$ gas flow) was shifted to 280 °C (in air flow). Moreover, the peak observed (at 280 °C) in flow of air was sharper than the one observed (at 390 °C) in flow of $N_2$ gas. This may indicate that nature of this step changes from decomposition into combustion in flow of $N_2$ gas or air, respectively.

Fig. 2 shows TGA and DTG curves of the dried 5% $CeO_2$/MCM-41 precursor in flow of $N_2$ atmosphere (top) and in flow of air (bottom). Total weight loss recorded upon heating over the temperature range of *RT*–700 °C was 25.5% in flow of $N_2$ flow (or 29.3% in flow of air). Similar to the above case of blank MCM-41, results show that the evolution of composite material also occurred through a four steps process, as shown in Table 1. The main weight loss steps for the removal of the tem-

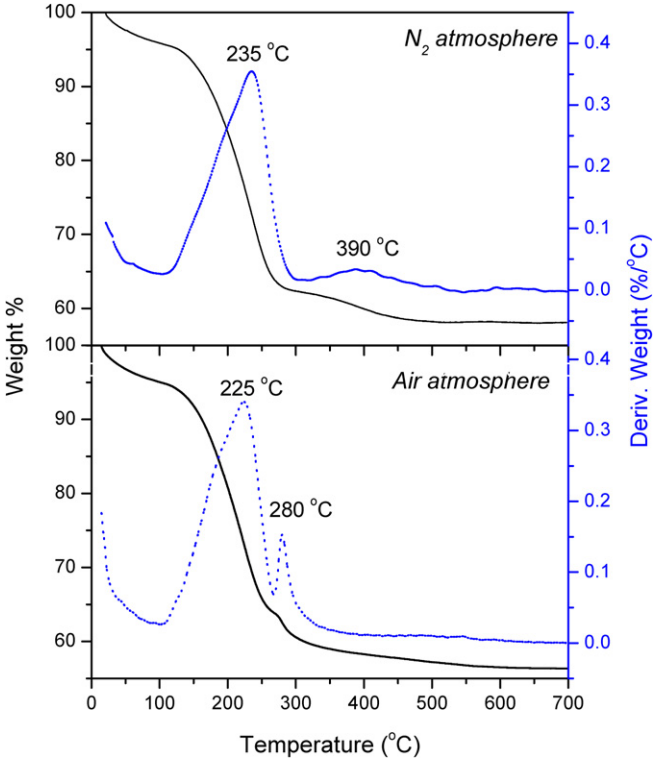


Fig. 1. TGA and DTG curves for the uncalcined blank MCM-41 material in flow of $N_2$ gas (top), and in flow of air (bottom).

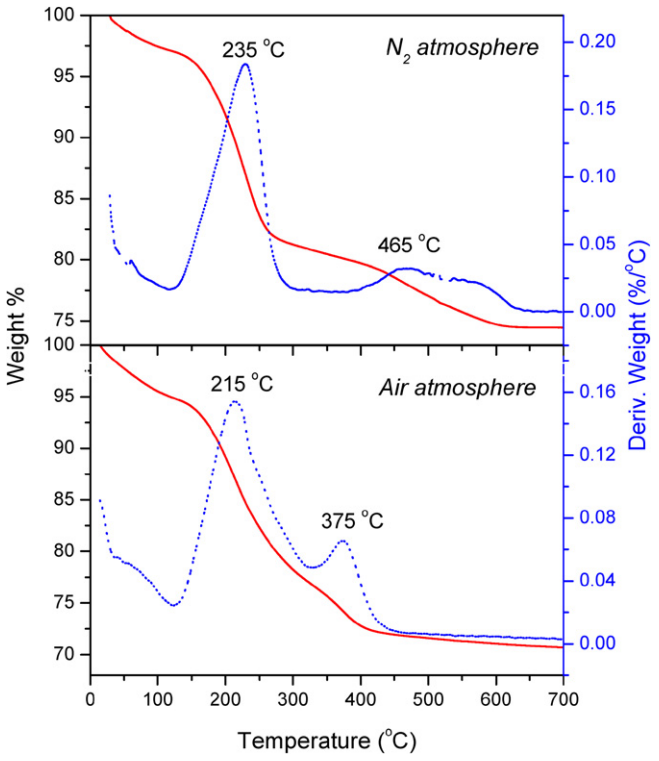


Fig. 2. TGA and DTG curves for the uncalcined 5% $CeO_2$/MCM-41 composite material in flow of $N_2$ gas (top), and in flow of air (bottom).

Table 1
TGA results for the uncalcined blank and 5% $CeO_2$/MCM-41 materials

| Samples | Temperature range (°C) | Δ weight loss (%) | Peak maximum (°C) |
|---|---|---|---|
| Blank MCM $N_2$ atmosphere | *RT*–105 | 4.3 | – |
| | 105–320 | 33.7 | 235 |
| | 320–550 | 3.8 | 390 |
| | 550–700 | <0.1 | – |
| | *RT*–700 | 41.9 | |
| Blank MCM air atmosphere | *RT*–125 | 5.1 | – |
| | 125–267 | 31.0 | 225 |
| | 267–400 | 5.6 | 280 |
| | 400–700 | 1.9 | – |
| | *RT*–700 | 43.6 | |
| 5% $CeO_2$/MCM $N_2$ atmosphere | *RT*–120 | 2.9 | – |
| | 120–330 | 16.3 | 235 |
| | 330–650 | 6.3 | 465 |
| | 650–700 | <0.05 | – |
| | *RT*–700 | 25.5 | |
| 5% $CeO_2$/MCM air atmosphere | *RT*–120 | 5.1 | – |
| | 120–325 | 18.0 | 215 |
| | 325–470 | 5.1 | 375 |
| | 470–700 | 1.1 | – |
| | *RT*–700 | 29.3 | |

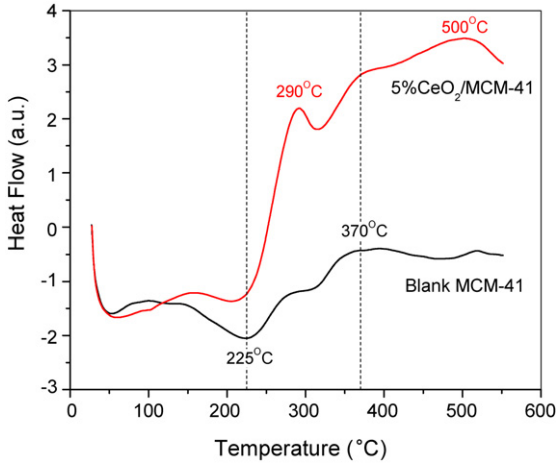


Fig. 3. DSC curves for the uncalcined blank MCM-41 and 5% $CeO_2$/MCM-41 composite materials in flow of $N_2$ gas, as indicated.

plate were characterize by two peaks at 235 and 465 °C in flow of $N_2$ atmosphere, (or at 215 and 375 °C in flow of air). However, in spite of the appearance of the former peak at about the same position observed for the blank MCM-41 (Fig. 1), position of the latter peak largely was delayed for the 5% $CeO_2$/MCM precursor to be at 465 °C (instead of 390 °C) in flow of $N_2$ atmosphere or delayed to 375 °C (instead of 280 °C) in flow of air atmosphere. This delay may be due to the interaction of some degradation products (from the previous decomposition steps) with cerium species and formation of some products which subsequently decompose and/or combust at higher temperatures.

DSC results for the analysis carried out at 10 °C/min in flow of $N_2$ for the blank MCM-41 and 5% $CeO_2$/MCM-41 atmosphere are shown in Fig. 3. For the blank MCM-41 precursor an endothermic peak was observed at 225 °C which followed by an exothermic one at 370 °C. These two peaks are in good agreement with the TGA peaks observed in flow of $N_2$ atmosphere (Fig. 1) which assigned for the two steps removal of the surfactant via Hofmann degradation at 235 °C, and decomposition and/or combustion reaction at 390 °C. The 5% $CeO_2$/MCM-41 precursor, as shown in Fig. 3, shows a related DSC profile that exhibiting an endothermic peak at 225 °C and an exothermic peak near 370 °C. This is in agreement with the TGA peaks observed in flow of $N_2$ atmosphere (Fig. 1a) and can be assigned as above. However, two additional exothermic peaks were observed at 290 and 500 °C, which are related to the presence of ceria.

Fig. 4 shows FTIR spectra for the uncalcined, Fig. 4 (top), and the calcined, Fig. 4 (bottom), materials. The spectrum for the uncalcined blank MCM-41 shows a group of strong intense bands at 3430, 2925, 2855, 1630, and 1475 $cm^{-1}$ and a group of bands in the region below 1400 $cm^{-1}$. The bands at 3430 and 1630 $cm^{-1}$ are assignable for to the starching and bending modes of adsorbed water molecules, the bands at 2925 and 2855 $cm^{-1}$ are assignable for the starching mode of $\nu CH(–CH_3)$ and $\nu CH(–CH_2–)$ groups [33,34], respectively. The band at 1475 $cm^{-1}$ is assignable for the bending mode of $\delta CH(–CH_3)$ and $\delta CH(–CH_2–)$ groups. The group of bands observed below 1400 $cm^{-1}$, is assignable for the framework vibration of Si-MCM-41 as shown below for the calcined materials. The spectrum obtained for the uncalcined 5% $CeO_2$/MCM-41 material, Fig. 4 (top), is similar to the spectrum obtained for the blank uncalcined material and confirms the inclusion of the template surfactant. Spectrum obtained for the uncalcined 10% $CeO_2$/MCM-41 material (not shown) was identical to the 5% $CeO_2$/MCM-41 and confirmed the inclusion of the template surfactant and showed no additional peaks.

FTIR spectra for the calcined materials are shown in Fig. 4 (bottom). The spectra show that the bands related to the template have been removed, and the remaining vibration bands are characteristic for MCM-41 type of materials [18,20,34]. Thus for the calcined blank MCM-41, spectrum a, as shown

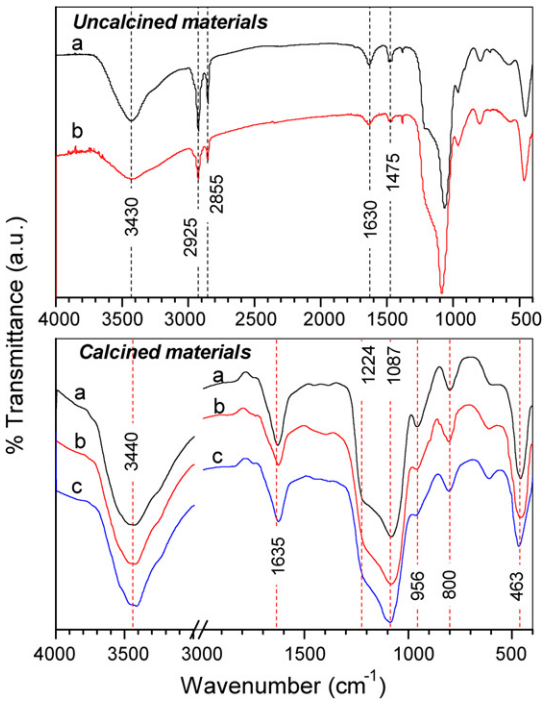


Fig. 4. FTIR spectra for the uncalcined materials (top) and the calcined materials (bottom) for (a) blank MCM-41 materials, (b) 5% $CeO_2$/MCM-41, and (c) 10% $CeO_2$/MCM-41.

in Fig. 4 (bottom), the bands at 3440 and 1635 $cm^{-1}$ are assigned to the starching and bending modes of adsorbed water molecules. The bands at 1224 and 1087 $cm^{-1}$ are assigned to $\nu_{as}$(Si–O–Si); the band at 956 $cm^{-1}$ is assigned to $\nu_{as}$(Si–OH); the band at 800 $cm^{-1}$ is assigned to $\nu_s$(Si–O–Si); and the band at 463 $cm^{-1}$ is assigned to $\delta$(Si–O–Si). For the calcined 5% $CeO_2$/MCM-41 composite material, Fig. 4 (bottom), similar group of vibration bands are observed. However, little shift toward smaller wavenumbers was recognized for the 3440, and 1635 $cm^{-1}$ bands, which can be taken as an indication for the insertion of $Ce^{4+}$ in the framework of Si-MCM-41 materials. Moreover, there is a change in the intensity of the 954 $cm^{-1}$ band, which indicates structural change for the surface Si–OH group due to the presence of $CeO_2$ species in the MCM-41 material, and/or due to evolution of a new vibration band, $\nu_{as}$(Si–O–Ce), which is due to manifest itself at the same position [18].

Diffuse reflectance UV–vis spectra of calcined blank and composite materials are shown in Fig. 5. The blank material showed no absorption over the examined wavelength range (200–800 nm) while, the $CeO_2$/MCM-41 composite materials showed one single band maximize at 290 nm. Moreover, intensity of this band increases on going from 5 to 10% $CeO_2$/MCM-41 composite, as shown in Fig. 5. In fact, DR UV–vis spectroscopy is known as a very sensitive probe for the characterization of metal ion coordination of metal containing zeolites. The position of ligand to metal charge transfer ($O^{2-} \rightarrow Ce^{4+}$) spectra depends on the ligand field symmetry surrounding the Ce center. Therefore, the technique gives valuable information about existence of the metal ions in the framework and/or in the extra framework position [18–20]. It its clear that the electronic transitions from oxygen to cerium require higher energy for a tetra-coordinated $Ce^{4+}$ ion than for a hexa-coordinated one (associated with $CeO_2$ species present at extra framework position), and therefore shorter wavelength (ca. 300 nm) should be observed for the former and longer wavelength (ca. 400 nm) should be expected for the latter [18]. Thus, it could be concluded that the presence of one absorption band at 290 nm for the $CeO_2$/MCM-41 composites is attributed to the presence of one type of well-dispersed $Ce^{4+}$ species (most likely) in a tetra-coordinated environment. It should be reported here that as a confirmation, a test sample was made to contain 20% $CeO_2$/MCM-41, and calcined as for the above composites (at 550 °C for 3 h). Diffuse reflectance UV–vis spectrum of this test sample (not shown) gave a band maximize at 290 nm, however a clear shoulder was observed at ∼360 nm.

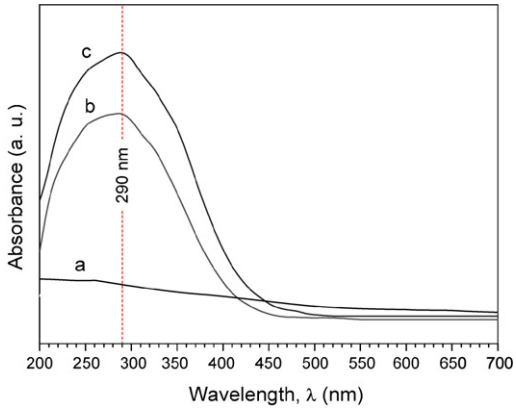


Fig. 5. Diffuse reflectance UV–vis spectra for the calcined materials as indicated, (a) blank MCM-41 materials, (b) 5% $CeO_2$/MCM-41, and (c) 10% $CeO_2$/MCM-41.

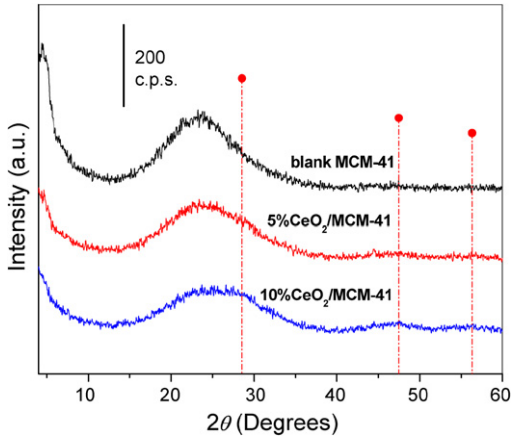


Fig. 6. XRD for the calcined materials as indicated.

XRD patterns for calcined materials, over the range of $2\theta = 4°$–$60°$, are shown in Fig. 6. The pattern obtained for the calcined MCM-41 silica, reflects the amorphous like nature of silica, which is normally obtained for MCM-41 materials in this $2\theta$ region [20]. Patterns for the calcined composites also, were dictated by the amorphous-like profile of silica. The pattern for the 5% $CeO_2$/MCM-41 materials shows no additional peaks, however, for the 10% $CeO_2$/MCM-41 composite, few weak broad peaks scarcely can be detected around positions of the

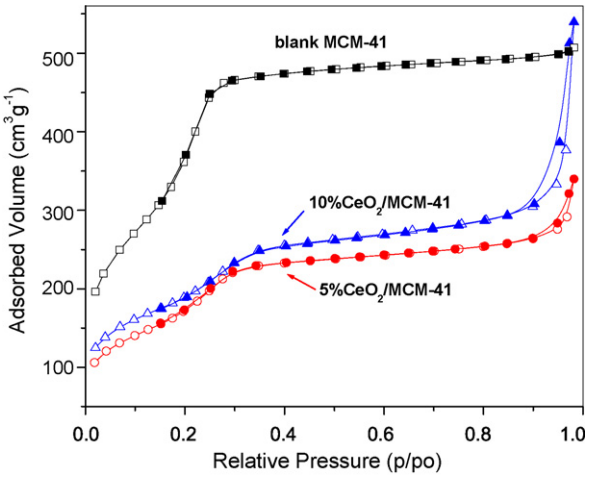


Fig. 7. Nitrogen adsorption/desorption isotherms for the different calcined materials as indicated (open symbols for adsorption and closed symbols for desorption).

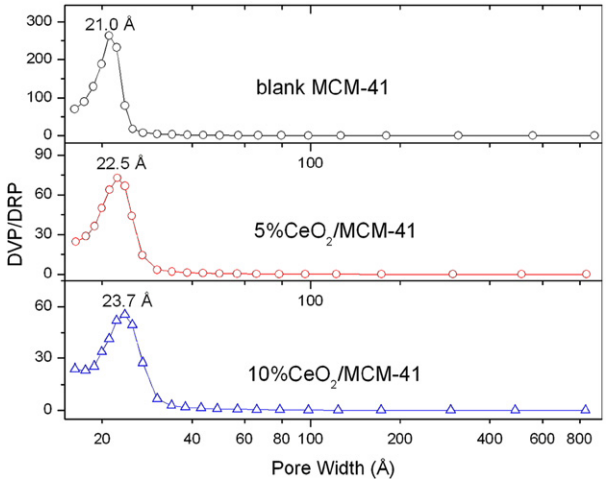


Fig. 8. BJH pore width distributions obtained with the different calcined materials as indicated.

Table 2
Surface area, $S_{BET}$; BET constant, $c_{BET}$; total pore volume, $V_p$; and average pore width, $P_w$ for the calcined materials

| Calcined material | $S_{BET}$ ($cm^3/g$) | $c_{BET}$ | $V_p$[a] ($m^2/g$) | $P_w$ (Å) |
|---|---|---|---|---|
| Blank MCM-41 | 1253 | 54 | 0.772 | 21.0 |
| 5% $CeO_2$/MCM-41 | 824 | 81 | 0.427 | 22.5 |
| 10% $CeO_2$/MCM-41 | 726 | 137 | 0.515 | 23.7 |

[a] Total pore volume was measured at $p/p_0 = 0.95$.

main characteristic lines for ceria at 28.55°, 47.47°, and 56.33°, respectively, which are corresponding to the (111), (220), and (311) planes of the cerianite (ceria) structure. These results indicate that finely, divided small nanosized cirea particles might be formed within the 10% $CeO_2$/MCM-41 composite. However, the very weak and broad nature of the observed ceria peaks for the 10% $CeO_2$/MCM-41 composites prevents any accurate estimation for the crystallite size to be done.

Nitrogen adsorption isotherms for the blank and composite MCM-41 calcined materials are shown in Fig. 7. The isotherm for the blank material can be classified as type IV type of isotherm, which is characteristic for MCM-41 materials [35]. Thus, at low $p/p_0$ values the isotherm show a linear increase of the adsorbed volume which is followed by a steep increase in nitrogen uptake at relative pressure range $0.20 < p/p_0 > 0.30$. This steep increase is indicative of capillary condensation inside the mesopores of small size (as shown by pore size distribution below). The long plateau at higher relative pressures indicates that there is no pore filling after $p/p_0 \geqslant 0.30$, i.e. at wider mesopores. Specific surface area amounts to 1253 $m^2/g$, was calculated for the blank material and further textural data are cited in Table 2.

Nitrogen adsorption isotherms for the calcined composite materials are shown in Fig. 7. The isotherms can be classified as type IV type of isotherms and show characteristics of MCM-41 type of materials; moreover, they are similar to isotherms normally observed for modified MCM-41 type of materials. Specific surface areas, $S_{BET}$, amount to 824 and 726 $m^2/g$, were calculated respectively for the 5 and 10% $CeO_2$/MCM-41 calcined composites. Total pore volume, $V_p$, amounting to 0.427 and 0.515 $cm^3/g$ respectively were obtained for the calcined 5 and 10% $CeO_2$/MCM-41 composites. The above results reveal an increasing adsorption at higher $p/p_0$ values, on going from 5 → 10% $CeO_2$/MCM-41 composite. This can be explained in terms of the increased open surfaces produced due to composite formation.

Pore width, $P_w$, distributions obtained with the calcined materials are shown in Fig. 8. For the calcined blank MCM-41 material a mono $P_w$ distribution maximize at 21.0 Å was obtained. Similar $P_w$ distributions were obtained with the 5 and 10% $CeO_2$/MCM-41 composite materials, which respectively maximize at 22.5 and 23.7 Å. This indicates that the insertion of cerium in the framework of MCM-41 led to little widening of porosity. Pore blockage was not a severe problem up to 10% $CeO_2$ loading and this can be explained in terms of the small particle size of the formed $CeO_2$ phase, and the pores (of MCM-41) themselves are short and nonintersecting.

SEM micrographs for the calcined blank MCM-41 along with the 10% $CeO_2$/MCM-41 composites are shown in Figs. 9a and 9b, respectively. Spherical particles formation was observed for the MCM-41 material, and this spherical morphology was preserved for the composite materials. No clear ceria aggregates were observed and this indicates that cerium was either inserted in the framework of MCM-41 and/or forms finely divided ceria particles on the wall of MCM-41 materials. Thus, indicating that effective dispersion of ceria on the very high surface area spherical MCM-41 material was achieved.

## 4. Conclusions

The above results confirm that the supporting functions of MCM-41 materials prepared via a nonhydrothermal method at room temperature is suitable for the direct preparation of high surface area $CeO_2$/MCM-41 composite materials of well organized porosity. The composites were found to preserve the characteristics of MCM-41 material and pore blockage was not severe for the 5% or even for 10% of $CeO_2$ loading.

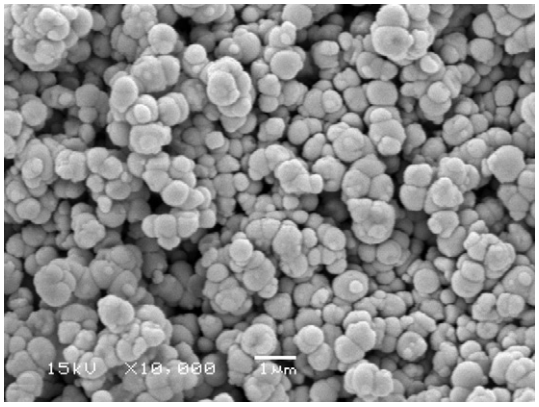


(a)

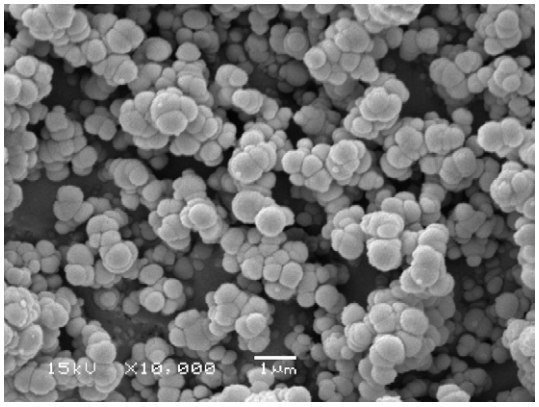


(b)

Fig. 9. SEM micrographs for the calcined (a) blank MCM-41 materials, and (b) 10% $CeO_2$/MCM-41 composite.

The present nonhydrothermal method takes the advantages of MCM-41, as a support, to stabilize $CeO_2$ particles, since the latter was not able to grow to larger size. Consequently, any formed particles were present inside pores and particle growth was limited because species movement to the external surface was hindered by the nonintersecting porous texture of the MCM-41 material. However, it should be kept in mined that the wall structure of MCM-41 type of material, as an ordered mesoporous silica material, rather resembles amorphous silica, i.e., shows no specific sites on the surface.

## References

[1] C.T. Kresge, M.E. Leonowicz, W.J. Roth, J.C. Vartuli, J.S. Beck, Nature 359 (1992) 710.
[2] J.S. Beck, J.C. Vartuli, W.J. Roth, M.E. Leonowicz, C.T. Kresge, K.D. Schmidt, C.T.-W. Chu, D.H. Olson, E.W. Sheppard, S.B. McCullen, J.B. Higgins, J.C. Schlenker, J. Am. Chem. Soc. 114 (1992) 10834.
[3] C.G. Sonwane, S.K. Bhatia, Langmuir 15 (1999) 2809.
[4] K. Cassiers, T. Linssen, M. Mathieu, M. Benjelloun, K. Schrijnemakers, P. Van Der Voort, P. Cool, E.F. Vansant, Chem. Mater. 14 (2002) 2317.
[5] A. Taguchi, F. Schüth, Micropor. Mesopor. Mater. 77 (2005) 1.
[6] A. Bourlinos, M.A. Karakassides, D. Petridis, J. Phys. Chem. B 104 (2000) 4375.
[7] M. Iwamoto, Y. Tanaka, J. Hirosumi, N. Kita, S. Triwahyono, Micropor. Mesopor. Mater. 48 (2001) 271.
[8] N. Lang, P. Delichere, A. Tuel, Micropor. Mesopor. Mater. 56 (2002) 203.
[9] P. Van Der Voort, E.F. Vansant, Micropor. Mesopor. Mater. 48 (2000) 385.
[10] P. Van Der Voort, M. Baltes, E.F. Vansant, Catal. Today 68 (2001) 119.
[11] A. Katovic, G. Giordano, B. Bonelli, B. Onida, E. Carrone, P. Lentz, J.B. Nagy, Micropor. Mesopor. Mater. 44–45 (2001) 275.
[12] H.-M. Lin, S.-T. Kao, K.-M. Lin, J.-R. Chang, S.-G. Shyu, J. Catal. 224 (2004) 156.
[13] M. Selvaraj, P.K. Sinha, K. Lee, I. Ahn, A. Pandurangan, T.G. Lee, Micropor. Mesopor. Mater. 78 (2005) 139.
[14] W. Lu, G. Lu, Y. Luo, A. Chen, J. Molec. Catal. A Chem. 188 (2002) 225.
[15] K.M.S. Khalil, L.A. Elkabee, B. Murphy, Micropor. Mesopor. Mater. 78 (2005) 83.
[16] K.M.S. Khalil, L.A. Elkabee, B. Murphy, J. Colloid Interface Sci. 287 (2005) 534.
[17] K.M.S. Khalil, J. Colloid Interface Sci. 307 (2007) 172.
[18] S.C. Laha, P. Mukherjee, S.R. Sainkar, R. Kumar, J. Catal. 207 (2002) 213.
[19] M.D. Kadgaonkar, S.C. Laha, R.K. Pandey, P. Kumar, S.P. Mirajkar, R. Kumar, Catal. Today 97 (2004) 225.
[20] W. Yao, Y. Chen, L. Min, H. Fang, Z. Yan, H. Wang, J. Wang, J. Molec. Catal. A Chem. 246 (2006) 162.
[21] A.S. Araujo, J.M.F.B. Aquino, M.J.B. Souza, A.O.S. Silva, J. Solid State Chem. 171 (2003) 371.
[22] M. Grün, K.K. Unger, A. Matsumoto, K. Tsutsumi, Micropor. Mesopor. Mater. 27 (1999) 207.
[23] A. Matsumoto, H. Chen, K. Tutsumi, M. Grün, K. Unger, Micropor. Mesopor. Mater. 32 (1999) 55.
[24] M.M.L. Ribeiro Carrott, F.L. Conceicao, J.M. Lopes, P.J.M. Carrott, C. Bernardes, J. Rocha, F. Ramoa Ribeiro, Micropor. Mesopor. Mater. 92 (2006) 270.
[25] T.N. Silva, J.M. Lopes, F. Ramoa Ribeiro, M.R. Carrott, P.C. Galacho, M.J. Sousa, P. Carrott, React. Kinet. Catal. Lett. 77 (2002) 83.
[26] C. Galacho, M.M.L. Ribeiro Carrott, P.J.M. Carrott, Micropor. Mesopor. Mater. 100 (2007) 312.
[27] A. Szegedi, M. Popova, V. Mavrodinova, M. Urban, I. Kiricsi, C. Minchev, Micropor. Mesopor. Mater. 99 (2007) 149.
[28] JCPDS, International Centre for Diffraction Data, PCPDFWIN, 1995, JCPDS-ICDD.
[29] K.S.W. Sing, D.H. Everett, R.A.W. Haul, L. Moscou, R.A. Pierotti, J. Rouquerol, T. Siemieniewska, Pure Appl. Chem. 57 (1985) 603.
[30] B. Brunauer, P.H. Emmett, P.H.E. Teller, J. Am. Chem. Soc. 60 (1938) 309.
[31] E.P. Barrett, L.G. Joyner, P.H. Halenda, J. Am. Chem. Soc. 73 (1951) 373.
[32] F. Kleitz, W. Schmidt, F. Schüth, Micropor. Mesopor. Mater. 65 (2003) 1.
[33] I.A. Degen, Tables of Characteristic Group Frequencies for the Interpretation of Infrared and Raman Spectra, Acolyte Publ., Harrow, UK, 1997.
[34] Y. Zheng, Z. Li, Y. Zheng, X. Shen, L. Lin, Mater. Lett. 60 (2006) 3221.
[35] F. Rouquerol, J. Rouquerol, K. Sing, Adsorption by Powders and Porous Solids, Academic Press, London, 1999, pp. 415–425.